Split electrons in partition density functional theory

Cite as: J. Chem. Phys. 156, 224113 (2022); https://doi.org/10.1063/5.0091024
Submitted: 10 March 2022 • Accepted: 22 May 2022 • Accepted Manuscript Online: 23 May 2022 • Published Online: 13 June 2022









ARTICLES YOU MAY BE INTERESTED IN

Density-functional theory vs density-functional fits

The Journal of Chemical Physics 156, 214101 (2022); https://doi.org/10.1063/5.0091198

Nuclear-electronic orbital approach to quantization of protons in periodic electronic structure calculations

The Journal of Chemical Physics 156, 224111 (2022); https://doi.org/10.1063/5.0088427

Finding critical points and reconstruction of electron densities on grids

The Journal of Chemical Physics 156, 224116 (2022); https://doi.org/10.1063/5.0090232

Lock-in Amplifiers up to 600 MHz



Zurich Instruments







Split electrons in partition density functional theory

Cite as: J. Chem. Phys. 156, 224113 (2022); doi: 10.1063/5.0091024

Submitted: 10 March 2022 • Accepted: 22 May 2022 •

Published Online: 13 June 2022









Kui Zhang¹ and Adam Wasserman^{1,2,a)}



AFFILIATIONS

- Department of Physics and Astronomy, Purdue University, West Lafayette, Indiana 47907, USA
- ²Department of Chemistry, Purdue University, West Lafayette, Indiana 47907, USA
- a) Author to whom correspondence should be addressed: awasser@purdue.edu

ABSTRACT

Partition density functional theory is a density embedding method that partitions a molecule into fragments by minimizing the sum of fragment energies subject to a local density constraint and a global electron-number constraint. To perform this minimization, we study a two-stage procedure in which the sum of fragment energies is lowered when electrons flow from fragments of lower electronegativity to fragments of higher electronegativity. The global minimum is reached when all electronegativities are equal. The non-integer fragment populations are dealt with in two different ways: (1) An ensemble approach (ENS) that involves averaging over calculations with different numbers of electrons (always integers) and (2) a simpler approach that involves fractionally occupying orbitals (FOO). We compare and contrast these two approaches and examine their performance in some of the simplest systems where one can transparently apply both, including simple models of heteronuclear diatomic molecules and actual diatomic molecules with two and four electrons. We find that, although both ENS and FOO methods lead to the same total energy and density, the ENS fragment densities are less distorted than those of FOO when compared to their isolated counterparts, and they tend to retain integer numbers of electrons. We establish the conditions under which the ENS populations can become fractional and observe that, even in those cases, the total charge transferred is always lower in ENS than in FOO. Similarly, the FOO fragment dipole moments provide an upper bound to the ENS dipoles. We explain why and discuss the

Published under an exclusive license by AIP Publishing. https://doi.org/10.1063/5.0091024

I. INTRODUCTION

Kohn-Sham Density Functional Theory (KS-DFT)¹⁻³ continues to be one of the most powerful and widely used methods to calculate the electronic properties of matter. Approximate exchange-correlation (XC) functionals used within KS-DFT suffer from various errors that limit their applicability.⁴ Among these errors, delocalization and static-correlation errors have been widely studied^{4,5} but, despite the several recent approaches to correct them,⁶⁻¹¹ there is still no general, robust method that works reliably in practice.

When dissociating a molecule into its constituent atoms, most approximate XC functionals will minimize the energy by placing fractional numbers of electrons on the separated atoms. The differences between these fractional numbers and the correct integers, referred to here as the "fractional-charge error" (FCE), are sometimes taken as a measure of the delocalization error (DE).¹² However, the DE, whose origin is the incorrect delocalization of electron densities, is not only present at dissociation. It is also present at any set of internuclear separations, for which the concept of "atomic electron number" is no longer valid (i.e., there is no unique way to assign electrons to any particular nucleus in the molecule). Although the FCE is only well defined at dissociation, one can show (see, for example, Fig. 2) that the error in the energy associated with the FCE settles in long before reaching dissociation when the "atoms" are still at interacting distances and their electronic densities cannot be understood separately. Theories that provide a definite prescription for calculating fragment populations at finite internuclear separations are thus useful in this context. 13-16

Various quantum embedding methods^{17,18} developed in recent years offer the possibility to invest most of the computational effort in specific fragments in a molecule while treating the remaining molecular framework (i.e., the "environment") as an electron bath with which electrons can be exchanged. Among such embedding methods, Partition-DFT (P-DFT)¹⁹⁻²¹ is particularly well suited to calculate fragment populations because, as will be discussed in Sec. II, it involves an energy minimization with respect to fragment populations. In other popular embedding methodologies, such as frozen-density embedding theory (FDET), 22-24 the fragment populations are usually kept fixed as integers. However, fractional electron populations have also been used by other embedding theories, usually through a method that involves fractionally occupying the KS orbitals (FOO) of the active fragment. 25-27 By contrast, most P-DFT calculations use an ensemble approach (ENS) that involves averaging over calculations with different numbers of electrons (always integers). 13,21 Although more computationally expensive than FOO, the ENS method shows advantages when describing intermolecular charge transfer.¹⁶ FOO and ENS are equivalent for the "exact" exchange-correlation functional, 28 but differ for approximate XC functionals as demonstrated numerically here. Although other methods to handle fractional fragment populations are conceivable, in this work, we compare and contrast the FOO and ENS approaches in P-DFT by using the Local Density Approximation (LDA) and examine their performance in some of the simplest systems where one can transparently apply both.

The long-term purpose of this line of research is three-fold: First, use P-DFT to improve the *accuracy* of approximate DFT calculations through physically motivated approximations to the partition energy, especially in systems with strong static or dynamic electron correlations where standard approximations to the exchange-correlation functional are limited; second, use P-DFT to exploit its potential linear-scaling implementations to improve the *efficiency* of calculations on systems of increasing complexity; and third, allow for calculations that, through their rigorous focus on *fragment* densities (as opposed to the *total* molecular density), can provide additional chemical insight that is missed by standard DFT. A clear prescription for the treatment of fractional charges is essential to make progress in all three directions. This work examines such prescription and clarifies how electrons can be split between fragments in P-DFT calculations.

All of the P-DFT calculations of fractional charges done to have been carried out on model systems of noninteracting^{14,30,31} or one-dimensional interacting³² electrons. Whenever 3D P-DFT calculations have involved fractional charges, the molecules studied have been centro-symmetric (homonuclear diatomics), not involving ground-state charge transfer between the constituent atoms. 21,33 We present here the first calculations on 3D heteronuclear diatomic molecules and ions. Our goal in this work is to examine how the two methods for splitting electrons between fragments (ENS and FOO) differ in practice. In Sec. II, we review the theory highlighting the role of electronegativity equalization and show how this important condition plays differently in FOO and ENS methods. In Sec. III, we present P-DFT calculations on 3D heteronuclear diatomic molecules with one, two, and four electrons, and show that, even though both ENS and FOO methods lead to the same total molecular densities, they lead to different descriptions of the charge transferred between fragments.

II. PARTITION-DFT AND TWO ALTERNATIVE METHODS FOR DETERMINING FRACTIONAL ELECTRON NUMBERS

To highlight the role of fractional populations in P-DFT, we begin with a description of P-DFT in which the $\{N_{\alpha}\}$ (α is used to

label fragments) are presumed fixed and known in advance. We will then describe how to optimize the set $\{N_{\alpha}\}$, but—as a first step—we consider these numbers as given, for example, by a calculation of formal charges from any of the many methods available for that purpose. $^{34-38}$

For a system of N_M electrons subject to an external potential $v(\mathbf{r})$ (due to all the nuclei), this potential can be divided as

$$v(\mathbf{r}) = \sum_{\alpha=1}^{N_f} v_{\alpha}(\mathbf{r}), \tag{1}$$

where $v_{\alpha}(\mathbf{r})$ is the external potential of the α th fragment and N_f is the number of fragments. The task of P-DFT is to minimize the sum of fragment energies,

$$E_f[\{n_\alpha\}] \equiv \sum_{\alpha=1}^{N_f} E_\alpha[n_\alpha], \tag{2}$$

subject to the set of constraints specified below [Eqs. (3) and (4)]. In Eq. (2), $E_{\alpha}[n_{\alpha}]$ and $n_{\alpha}(\mathbf{r})$ are the ground-state energy and density of the α th fragment, respectively. Given a set $\{N_{\alpha}\}$ satisfying $\sum\limits_{\alpha=1}^{N_f} N_{\alpha} = N_M$, where the total number of electrons N_M is an integer, the total ground-state density $n_M(\mathbf{r})$ is optimally partitioned when E_f is minimized with respect to variations of the $\{n_{\alpha}\}$ subject to the N_f+1 independent constraints,

$$n_M(\mathbf{r}) = \sum_{\alpha=1}^{N_f} n_\alpha(\mathbf{r}), \tag{3}$$

$$N_{\alpha} = \int n_{\alpha}(\mathbf{r}) d\mathbf{r}, \ \forall \alpha \in \{1, \dots, N_f\}.$$
 (4)

Because the N_{α} can be non-integer, $E_{\alpha}[n_{\alpha}]$ needs to be defined for non-integer electron numbers. Two alternative methods for accomplishing this are described in Secs. II A and II B. In either case, the constrained search for an optimum $\{n_{\alpha}\}$ for fixed $\{N_{\alpha}\}$ can be formally converted into the unconstrained minimization of a grand-potential $G[\{n_{\alpha}\}, v_{p}(\mathbf{r}), \{\chi_{\alpha}\}]$, where the partition potential $v_{p}(\mathbf{r})$ and fragment electronegativities $\{\chi_{\alpha}\}$ are the Lagrange multipliers associated with constraints (3) and (4), respectively,

$$G[\{n_{\alpha}\}, \nu_{p}(\mathbf{r}), \{\chi_{\alpha}\}] = E_{f}[\{n_{\alpha}\}] + \int \nu_{p}(\mathbf{r})$$

$$\times \left(\sum_{\alpha} n_{\alpha}(\mathbf{r}) - n_{M}(\mathbf{r})\right) d\mathbf{r}$$

$$+ \sum_{\alpha} \chi_{\alpha} \left(\int n_{\alpha}(\mathbf{r}) d\mathbf{r} - N_{\alpha}\right). \tag{5}$$

The Euler–Lagrange equation for the α th fragment can be obtained by minimizing $G[\{n_{\alpha}\}, \nu_{p}(\mathbf{r}), \{\chi_{\alpha}\}]$ with respect to the corresponding fragment density $n_{\alpha}(\mathbf{r})$, i.e., $\frac{\delta G}{\delta n_{\alpha}(\mathbf{r})} = 0$, yielding

$$\chi_{\alpha} = -\left(\frac{\delta E_{\alpha}[n_{\alpha}]}{\delta n_{\alpha}(\mathbf{r})} + \nu_{p}(\mathbf{r})\right),\tag{6}$$

where $\frac{\delta E_\alpha[n_\alpha]}{\delta n_\alpha(\mathbf{r})}$ needs to be well defined for non-integer electron numbers (see Secs. II A and II B).

The $v_p(\mathbf{r})$ for fixed $\{N_\alpha\}$ is unique, ^{13,19,26} but E_f can generally be lowered further by transferring a fraction of an electron from a fragment of lower electronegativity to one of higher electronegativity. The global minimum of E_f is then found when all fragment electronegativities are equal, ^{13,19} i.e., $\chi_{\alpha} = \chi^*, \forall \alpha$, where χ^* is a common optimal electronegativity. Then, the constraints (4) unify into

$$N_M = \sum_{\alpha=1}^{N_f} \int n_{\alpha}(\mathbf{r}) d^3 \mathbf{r}, \tag{7}$$

and the grand potential $G[\{n_{\alpha}\}, \nu_{p}(\mathbf{r}), \{\chi_{\alpha}\}]$ becomes

$$G[\{n_{\alpha}\}, \nu_{p}(\mathbf{r}), \chi^{*}] = E_{f}[\{n_{\alpha}\}] + \int \nu_{p}(\mathbf{r})$$

$$\times \left(\sum_{\alpha} n_{\alpha}(\mathbf{r}) - n_{M}(\mathbf{r})\right) d^{3}\mathbf{r}$$

$$+ \chi^{*}\left(\sum_{\alpha} \int n_{\alpha}(\mathbf{r}) d^{3}\mathbf{r} - N_{M}\right), \qquad (8)$$

with
$$\chi^* = -\left(\frac{\delta E_f[\{n_\alpha\}]}{\delta n_M(\mathbf{r})} + \nu_p(\mathbf{r})\right)$$

with $\chi^* = -\left(\frac{\delta E_f[\{n_\alpha\}]}{\delta n_M(\mathbf{r})} + \nu_p(\mathbf{r})\right)$. Thus, by varying the $\{N_\alpha\}$, we can determine the optimal fragment electron populations for which all fragment electronegativities are equal and the grand-potential is minimized to

$$E_f^* = \min_{\substack{\{\gamma_\alpha\} \ \{n_\alpha\}}} \min_{\substack{\{\gamma_\alpha\} \ \{n_\alpha\}}} G[\{n_\alpha\}, \nu_p(\mathbf{r}), \{\chi_\alpha\}]. \tag{9}$$

A general, simple algorithm for Eq. (9) can be formulated: Start with a guess for $\{N_{\alpha}\}$ and do self-consistent calculations to obtain all fragment electronegativities $\{\chi_{\alpha}\}$. Then, update the $\{N_{\alpha}\}$ by using $N_{\alpha}^{(k+1)} = N_{\alpha}^{(k)} + \Gamma(\chi_{\alpha}^{(k)} - \bar{\chi}^{(k)})$, where Γ is an appropriate positive constant and $\bar{\chi}^{(k)}$ is the average of all fragment electronegativities for the kth iteration. The process is iterated until $\chi_{\alpha}^{(k)} - \bar{\chi}^{(k)}$ falls below an acceptable threshold. The resulting $\{N_{\alpha}\}$ will be referred to as *optimal* and be denoted as $\{N_{\alpha}^{*}\}$ from now on. We now turn our attention to two alternative methods for treating non-integer electron numbers.

A. Fractional orbital occupations (FOO)

The density of the α th fragment can be constructed as

$$n_{\alpha}^{\text{FOO}}(\mathbf{r}) = \sum_{i} f_{\alpha,i} |\phi_{\alpha,i}(\mathbf{r})|^{2},$$
 (10)

where $\sum f_{\alpha,i} = N_{\alpha}$, and $f_{\alpha,i}$ is the occupation number for $\phi_{\alpha,i}(\mathbf{r})$ (the ith KS orbital of the α th fragment). Since we only consider the ground state, $f_{\alpha,i} = 1$ for all occupied orbitals except for the highest occupied molecular orbital (HOMO), in which case $0 < f_{\alpha}^{\text{HOMO}} \le 1$. The non-interacting kinetic energy is calculated by³⁹

$$T_s^{\text{FOO}}[n_{\alpha}] = -\frac{1}{2} \sum_{i} f_{\alpha,i} \int \phi_{\alpha,i}^*(\mathbf{r}) \nabla^2 \phi_{\alpha,i}(\mathbf{r}) d\mathbf{r}. \tag{11}$$

The energy of the α th fragment $E_{\alpha}[n_{\alpha}]$ is then defined in the same way as in KS-DFT (we drop the "FOO" superscript from the densities for notational simplicity),

$$E_{\alpha}[n_{\alpha}] = T_{s}^{\text{FOO}}[n_{\alpha}] + E_{\text{HXC}}[n_{\alpha}] + \int v_{\alpha}(\mathbf{r}) n_{\alpha}(\mathbf{r}) d\mathbf{r}, \qquad (12)$$

where $E_{\rm H}[n_{\alpha}]$ and $E_{\rm XC}[n_{\alpha}]$ are the Hartree and exchangecorrelation energies of the ath fragment, respectively. Then, the Euler-Lagrange equation (6) becomes

$$\chi_{\alpha}^{\text{FOO}} = -\left(\frac{T_s^{\text{FOO}}[n_{\alpha}]}{\delta n_{\alpha}(\mathbf{r})} + \nu_{\text{HXC}}[n_{\alpha}](\mathbf{r}) + \nu_{\alpha}(\mathbf{r}) + \nu_{p}(\mathbf{r})\right). \tag{13}$$

In the same way as in KS-DFT,3 one can derive the KS equations for the α th fragment,

$$\left\{-\frac{1}{2}\nabla^2 + \nu_{\alpha}^{\text{eff}}[n_{\alpha}](\mathbf{r}) + \nu_{p}(\mathbf{r})\right\}\phi_{\alpha,i}(\mathbf{r}) = \varepsilon_{\alpha,i}\phi_{\alpha,i}(\mathbf{r}), \quad (14)$$

where the fragment effective potential is

$$v_{\alpha}^{\text{eff}}[n_{\alpha}](\mathbf{r}) = v_{\alpha}(\mathbf{r}) + v_{\text{HXC}}[n_{\alpha}](\mathbf{r}). \tag{15}$$

The fragment KS equations for the ath fragment can be regarded as those for N_{α} electrons subject to the external potential $v_{\alpha}(\mathbf{r}) + v_{p}(\mathbf{r})$. Therefore, we define the total energy for the α th fragment as

$$\widetilde{E}_{\alpha}[n_{\alpha}] \equiv E_{\alpha}[n_{\alpha}] + \int \nu_{p}(\mathbf{r}) n_{\alpha}(\mathbf{r}) d\mathbf{r}.$$
 (16)

Considering that N_{α} is continuous and the energy is differentiable, we use the definition of electronegativity given by Iczkowski and Margrave, 40 i.e., $\chi_{\alpha}=-\frac{\partial\widetilde{E}_{\alpha}}{\partial N_{\alpha}}$. It is straightforward to prove that the energy functional $\widetilde{E}_{\alpha}[n_{\alpha}]$ is differentiable^{41,42} and $\chi_{\alpha}^{FOO} = -\frac{\delta \widetilde{E}_{\alpha}[n_{\alpha}]}{\delta n_{\alpha}(\mathbf{r})}$ = $-\frac{\partial \widetilde{E}_{\alpha}}{\partial N_{\alpha}}$. $^{3.43}$ Furthermore, according to Janak's theorem, 39 we know that $\frac{\partial \widetilde{E}_{\alpha}}{\partial N_{\alpha}} = \varepsilon_{\alpha}^{HOMO}$. Thus, we obtain $\chi_{\alpha}^{FOO} = -\varepsilon_{\alpha}^{HOMO}$.

B. Ensembles (ENS)

Alternatively, when N_{α} lies between the integers p_{α} (= $\lfloor N_{\alpha} \rfloor$) and p_{α} + 1, we can write the α -density as

$$n_{\alpha}^{\text{ENS}}(\mathbf{r}) = (1 - \omega_{\alpha}) n_{p_{\alpha}}(\mathbf{r}) + \omega_{\alpha} n_{p_{\alpha}+1}(\mathbf{r}), \tag{17}$$

emulating known results for the exact extension of DFT to noninteger electron numbers²⁸ (true for the exact XC-functional). A related approach⁷ has been shown to be useful in eliminating the asymptotic fractional dissociation problem of the LDA. In Eq. (17), the two ensemble component densities $n_{p_{\alpha}}(\mathbf{r})$ and $n_{p_{\alpha+1}}(\mathbf{r})$ integrate to p_{α} and p_{α} + 1 electrons, respectively, and $0 < \omega_{\alpha} < 1$ so that $N_{\alpha} = p_{\alpha} + \omega_{\alpha}$.

The corresponding fragment energy is

$$E_{\alpha}[n_{\alpha}] = (1 - \omega_{\alpha})E_{\alpha}[n_{p_{\alpha}}] + \omega_{\alpha}E_{\alpha}[n_{p_{\alpha}+1}], \tag{18}$$

where $E_{\alpha}[n_{p_{\alpha}}]$ and $E_{\alpha}[n_{p_{\alpha}+1}]$ are, respectively, the ground-state energies for p_{α} and $p_{\alpha}+1$ electrons subject to an external potential $v_{\alpha}(\mathbf{r}) + v_{p}(\mathbf{r})$.

Since the allowed density variations must now keep p_{α} electrons in $n_{p_{\alpha}}(\mathbf{r})$ and $p_{\alpha}+1$ electrons in $n_{p_{\alpha}}+1(\mathbf{r})$, the constraints (4) turn into $2N_f$ independent constraints, and the Lagrange multipliers $\{\chi_{\alpha}\}$ can be replaced by a pair-set of multipliers $\{\lambda_{p_{\alpha}},\lambda_{p_{\alpha}+1}\}$. The grand-potential in Eq. (5), now $G^{\text{ENS}}[\{n_{\alpha}\},v_p(\mathbf{r}),\{\lambda_{p_{\alpha}},\lambda_{p_{\alpha}+1}\}]$, is minimized with respect to variations in the $n_{p_{\alpha}}(\mathbf{r})$ and $n_{p_{\alpha}}+1(\mathbf{r})$, yielding

$$\lambda_{p_{\alpha}} = -\left(\frac{\delta E_{\alpha}[n_{p_{\alpha}}]}{\delta n_{p_{\alpha}}(\mathbf{r})} + \nu_{p}(\mathbf{r})\right),\tag{19}$$

and a companion equation for $\lambda_{p_\alpha+1}$. Expressing $E_\alpha[n_{p_\alpha}]$ in terms of KS quantities, Eq. (14) is now replaced by a pair of analogous KS equations in which all of the α -subindices in Eq. (14) are replaced by either p_α or $p_\alpha+1$. The fragment effective potential $v_{p_\alpha}^{\rm eff}[n_{p_\alpha}](\mathbf{r})$ has the same decomposition as in Eq. (15), but the Hartree and XC-potentials are now evaluated at the appropriate integer-number densities. These in turn are constructed simply by summing over the p_α (or $p_\alpha+1$) occupied KS orbitals.

 p_{α} (or $p_{\alpha}+1$) occupied KS orbitals. For atoms and molecules, $\varepsilon_{p_{\alpha}}^{\mathrm{HOMO}}<\varepsilon_{p_{\alpha}+1}^{\mathrm{HOMO}}$ and $\lambda_{p_{\alpha}}>\lambda_{p_{\alpha}+1}$, since the p_{α} and $p_{\alpha}+1$ electrons are subjected to the same external potential $v_{\alpha}(\mathbf{r})+v_{p}(\mathbf{r})$. Defining the total energy for the α th fragment in the same way as Eq. (16), we now find for the electronegativity, ²⁸

$$\chi_{\alpha}^{\rm ENS} = \widetilde{E}_{\alpha}[n_{p_{\alpha}}] - \widetilde{E}_{\alpha}[n_{p_{\alpha}+1}] \qquad (0 < \omega_{\alpha} < 1). \tag{20}$$

If N_{α} is an integer, $\chi_{\alpha}^{\text{ENS}}$ is strictly undefined (but one can consider right- and left-limits for it, as will be discussed in Sec. III B).

C. HOMO energy and electronegativity: FOO vs ENS

The one-electron nature of the KS equations leads to densities for finite systems that decay asymptotically as 3,44

$$n(\mathbf{r}) \xrightarrow[r \to \infty]{} e^{-2\kappa r},$$
 (21)

where $\kappa = \sqrt{-2(\varepsilon^{\text{HOMO}} - \nu_{\text{XC}}(\infty))}$. If $\nu_{\text{XC}}(\mathbf{r}) \xrightarrow[r \to \infty]{} 0$, then $\kappa = \sqrt{-2\varepsilon^{\text{HOMO}}}$. LDA and GGA densities satisfy this condition.

Due to the density constraint of Eq. (3), we see that if the fragment densities have different exponential decay rates, at least one of them (fragment α^*) must match the decay of the total density in the asymptotic region. Using FOO, this implies $\varepsilon_{\alpha^*}^{\rm HOMO}=\varepsilon_M^{\rm HOMO}=const.$ By using $\chi_{\alpha}^{\rm FOO}=-\varepsilon_{\alpha}^{\rm HOMO}$ (see the last line of Sec. II A), we find that $\chi_{\alpha^*}^{\rm FOO}=-\varepsilon_M^{\rm HOMO}$. When E_f reaches its global minimum, all fragment electronegativities are equal, so $\chi_{\alpha}=-\varepsilon_M^{\rm HOMO}$ for all α . Therefore, the best way to approach the global minimum of E_f is to always assign less electrons to fragments whose electronegativities are χ_M and more electrons to fragments whose electronegativities are larger than χ_M . In this way, the iteration formula in the algorithm for

Eq. (9) can be modified for the (k+1)th iteration as follows: For fragments whose $\chi_{\alpha}^{(k)} > \chi_{M}$, set $N_{\alpha}^{(k+1)} = N_{\alpha}^{(k)} + \Gamma(\chi_{\alpha}^{(k)} - \chi_{M})$; for fragments whose $\chi_{\alpha}^{(k)} = \chi_{M}$, set $N_{\alpha}^{(k+1)} = N_{\alpha}^{(k)}$ or $N_{\alpha}^{(k+1)} = N_{M} - \sum_{\beta \neq \alpha} N_{\beta}^{(k)}$.

In contrast, when using the ENS method of Sec. II B, we find $\varepsilon_{p_{\alpha^*+1}}^{\text{HOMO}} = \varepsilon_M^{\text{HOMO}} = \text{const}$, and there is no direct relation between the fragment electronegativity $\chi_{\alpha}^{\text{ENS}}$ of Eq. (20) and the molecular HOMO energy.

Finally, we note a key difference between the partition potentials of ENS and FOO: Assume the population of the \$\alpha\$th fragment is a non-integer and \$\varepsilon_{\alpha, FOO}^{HOMO} = \varepsilon_M^{HOMO}\$, then we know \$\varepsilon_{\alpha, ENS}^{HOMO} \leq \varepsilon_M^{HOMO}\$. Since there are \$N_{\alpha}\$ electrons subject to \$v_{\alpha}(\mathbf{r}) + v_p^{FOO}(\mathbf{r})\$ in FOO, while there are \$|N_{\alpha}| + 1\$ electrons subject to \$v_{\alpha}(\mathbf{r}) + v_p^{ENS}(\mathbf{r})\$ in ENS, \$v_p^{ENS}(\mathbf{r})\$ needs to be deeper than \$v_p^{FOO}(\mathbf{r})\$ to account for the fact that \$|N_{\alpha}| + 1 > N_{\alpha}\$, and thus \$\int v_p^{ENS}(\mathbf{r}) n_M(\mathbf{r}) d\mathbf{r} < \int v_p^{FOO}(\mathbf{r}) n_M(\mathbf{r}) d\mathbf{r}\$. As a consequence, \$E_p^{ENS}\$ is more negative than \$E_p^{FOO}\$ and, since FOO and ENS must yield the same total energy, \$E_f^{ENS}\$ will be less negative than \$E_f^{FOO}\$. All of these findings are illustrated below.

III. EXAMPLES AND DISCUSSION

We now illustrate the preceding discussions on a few model systems of diatomic molecules that have been used in other contexts 30,45,46 and on actual diatomic molecules. In all cases, the nuclei are separated by a distance R and located at $-(R/2)\hat{z}$ and $+(R/2)\hat{z}$ along the z-axis. All calculations are performed on a prolate-spheroidal real-space grid. 21,47 Considering the azimuthal symmetry of diatomic molecules, we only need to solve the Kohn–Sham equations on a two-dimensional mesh. Libxc library 48 is used to evaluate approximate exchange–correlation functionals.

We partition the molecules into two fragments, labeled A and B, and denote the *optimal* electron populations by N_A^* and N_B^* . When isolated $(R \to \infty)$, the correct populations are denoted by N_A^0 and N_B^0 , so we can define the number of electrons transferred from A to B as $\Delta N = N_A^0 - N_A^* = N_B^* - N_B^0$. When no superscript is used for N_A and N_B , it should be understood that the numbers have been fixed, but not optimized (i.e., they do not minimize E_f).

A. One electron: Model of a one-electron molecule $\mathbf{A}\mathbf{B}^{+\mathbf{Z}_B}$

We first consider a one-electron diatomic molecular ion AB^{+Z_B} with nuclear charges $Z_A = 1$ and variable $Z_B < 1$, so that the dissociated molecule consists of a hydrogen atom and a "proton" of charge $+Z_B$. (In the discussion below, we sometimes refer to $\Delta Z \equiv 1 - Z_B$.) A similar model but in 1D and with delta-function potentials was studied in Ref. 30. We take $E_{XC}^{EXACT}[n] = -E_H[n]$ as the exact functional for the one-electron system. The *exact* P-DFT solution reported here for Coulomb potentials in 3D leads to well-localized fragment densities for all R (see Fig. 1), just like in the 1D model of Ref. 30. As the molecule is stretched, an electron is smoothly transferred from B to A. (What we mean by "smoothly" will be clarified below; see the right panel of Fig. 2.)

The left panel of Fig. 2 compares the *exact* and LDA dissociation curves of AB^{+Z_B} , showing a vivid example of LDA fractional-charge and delocalization errors. The equilibrium distance R_{eq} is

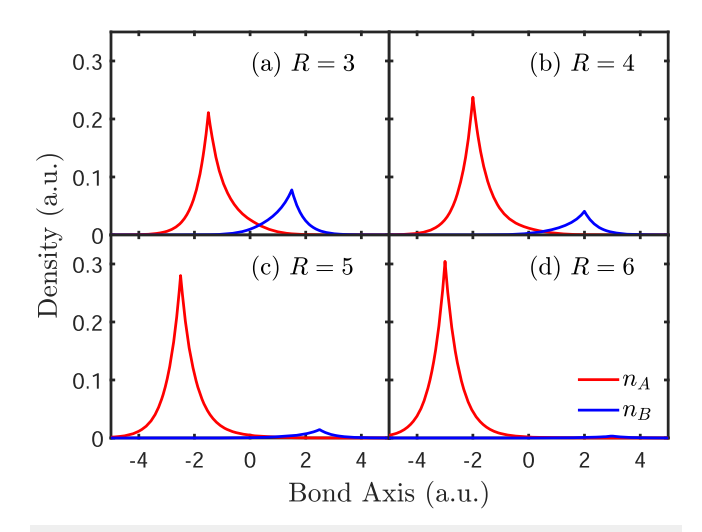


FIG. 1. The optimal electron densities of fragments along the bond axis for model molecule $AB^{+0.9}$ ($Z_A = 1$ and $Z_B = 0.90$) with the exact functional when the internuclear distance is (a)–(d) R = 3.0, 4.0, 5.0, and 6.0 a.u., respectively.

about 2 a.u. for the exact solution and about 2.3 a.u. for the LDA (R_{eq} is approximately constant in the range 0.9 < Z_B < 1). Two lessons can be drawn from the left panel of Fig. 2:

- (1) The bond is stronger for the homonuclear case than it is for the heteronuclear case. The larger the value of ΔZ , the weaker the binding, as explained beautifully in Chapter 10 of Ref. 49.
- (2) The LDA error manifests most clearly at the dissociation limit as the binding energy E_b goes incorrectly to a negative value (E_b is defined as the difference between the ground-state energy of the molecule and the sum of the ground-state energies of the isolated atoms, in this case just a hydrogen atom, so should be zero at dissociation). Furthermore, Fig. 2

shows that this error increases as $\Delta Z \to 0$. In the limiting case of $\Delta Z = 0$ (i.e., H_2^+), the error has been well studied and understood as due to the incorrect treatment of fractional charges by the LDA. A hallmark of the delocalization error (DE) for a heteronuclear diatomic molecule is that the approximate functional incorrectly minimizes the total energy by placing fractional charges on the separated atoms. These incorrect fractional charges are well defined at dissociation. An interesting question arises here: The (incorrect) fractional charges that determine the DE are strictly only well defined at dissociation, as mentioned in Sec. I, but the left panel of Fig. 2 shows that the DE settles in slowly as $R \gtrsim 4$. How do the fractional charges at *finite R* evolve into those at dissociation as $R \to \infty$?

The right panel of Fig. 2 provides the answer given by Partition-DFT through both ENS and FOO methods described in Sec. II, using both the exact functional and the LDA. For the exact case, ENS and FOO fragments are identical. The number of electrons in the B-fragment (N_B) reaches a maximum value for small R and decreases monotonically down to zero at dissociation in the same way as was observed for the 1D model system of Ref. 30. However, in the case of an approximate functional such as the LDA, although FOO and ENS yield the same total molecular density and energy, they yield different fragment energies and densities. The ENS-LDA N_B values are close to the exact ones for very small internuclear separations and around the maximum of N_B , but they do not decrease as R grows and stay approximately constant for $R \gtrsim 4$, suggesting that the error in N_B encodes the error in E_b . The FOO-LDA N_B values converge to those of ENS-LDA as R grows, but differ significantly for small *R*.

To discuss the origin of these differences, we take the case of $Z_B = 0.9$ as an example and fix R = 2.0 a.u. (close to equilibrium).

1. FOO

The LDA electronegativities χ_A and χ_B , as defined below Eq. (16), become equal when N_A^* = 0.5830 (for the exact case, they

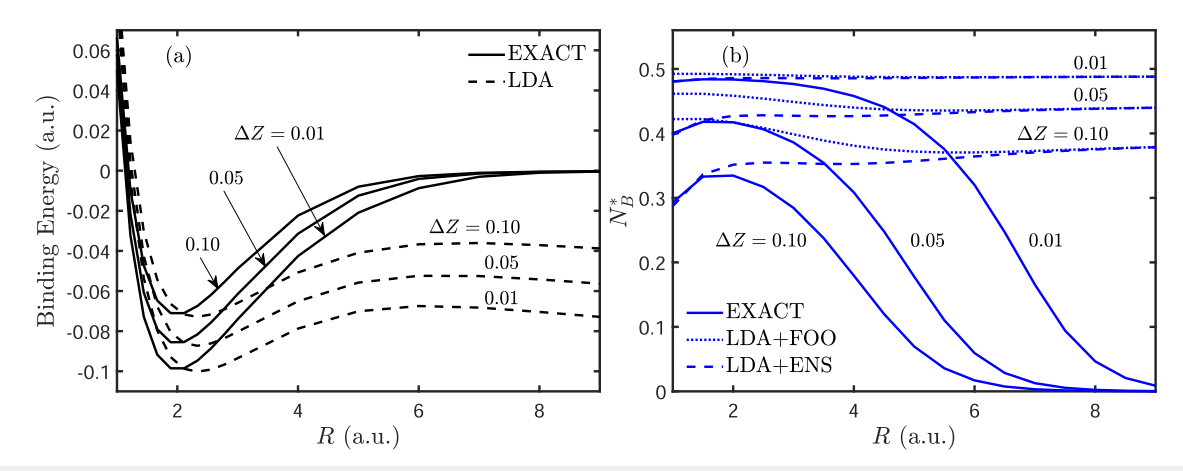


FIG. 2. (a) Binding energies for the model of a one-electron heteronuclear diatomic molecule AB^{+Z_B} (Sec. III A) with the exact functional (solid) and the LDA (dashed) for $Z_A = 1$, and $Z_B = 0.90, 0.95, 0.99$. (b) Corresponding optimal population of fragment B. FOO and ENS results lead to identical binding energies, but their corresponding N_B^* differ when using the LDA.

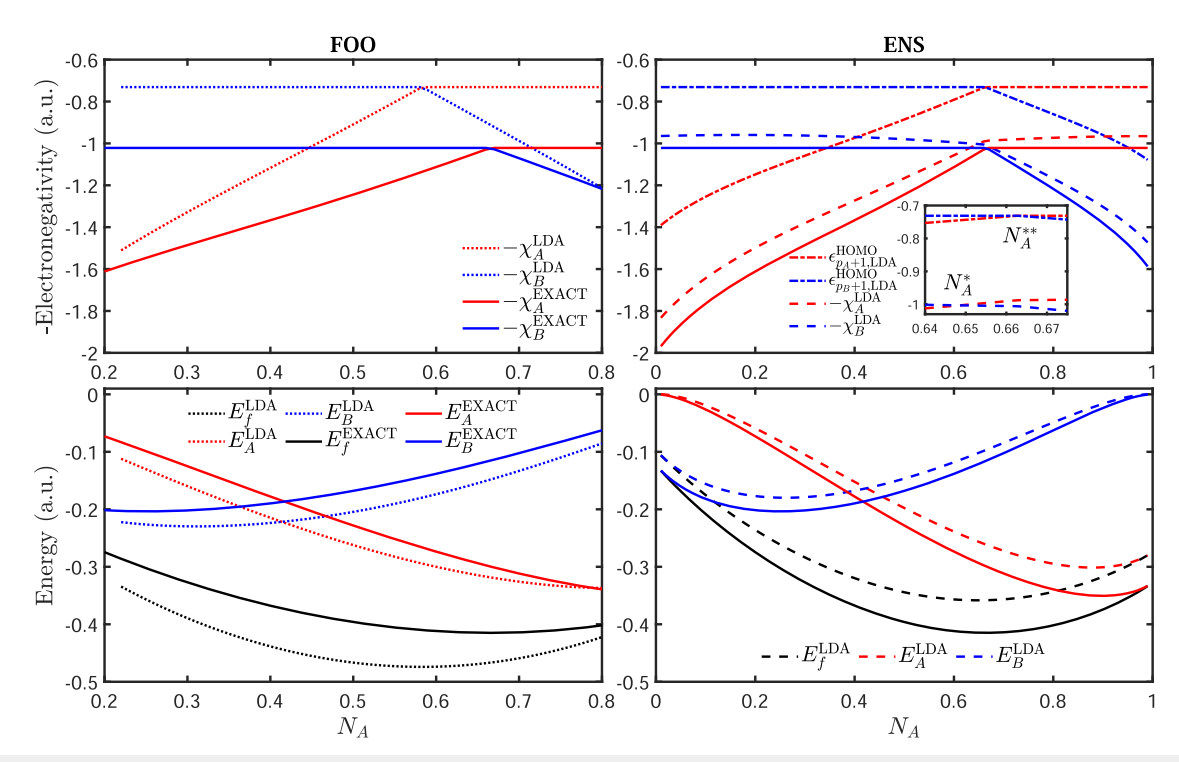


FIG. 3. Negative electronegativities of fragments (top panels) and fragment energies and their sum (bottom panels) as a function of N_A for the one-electron model molecule AB^{+0.9} of Sec. III A ($Z_A = 1$ and $Z_B = 0.9$; at internuclear distance R = 2.0 a.u., $\varepsilon_{M,\mathrm{LDA}}^{\mathrm{HOMO}} = -0.7311$ a.u., and $\varepsilon_{M,\mathrm{EXACT}}^{\mathrm{HOMO}} = -1.0216$ a.u.) with LDA and exact functionals. Left panels: FOO. Right panels: ENS.

equalize at $N_A^*=0.6654$, so the LDA error for the optimum occupation is -12%). This number is also the minimizer of E_f (see the bottom panels of Fig. 3). When $N_A < N_A^*$, the electronegativity of B equals $-\varepsilon_M^{\rm HOMO}$, a constant value. In this range, $\chi_A > \chi_B$, so fragment A has a higher tendency than B to attract electrons—B is the donor ("base") and A is the acceptor ("acid"). As electrons are transferred from B to A, both the electronegativity difference $\chi_A - \chi_B$ and E_f decrease. On the other hand, when $N_A > N_A^*$, fragments A and B swap their donor/acceptor roles.

2. ENS

The LDA electronegativities now cross at $N_A^* = 0.6485$. By switching from FOO to ENS, the magnitude of the error in N_A^* has thus been reduced from 12% to 2%. The HOMO energy of the molecule equals the HOMO energy of one of the two fragments. That fragment is A when $N_A > N_A^{**}$ and B when $N_A < N_A^{**}$, where N_A^{**} is the crossing point of the fragment HOMO energies, which differs slightly from N_A^* (the crossing point for the electronegativities). In the case of Fig. 3 (see the inset in the top right panel), $N_A^{**} = 0.6630$.

This example indicates that the FOO method leads to a larger estimate than ENS for the charge transferred. In the case of Fig. 3, $\Delta N^{\rm FOO}=0.4170$ and $\Delta N^{\rm ENS}=0.3515$.

Now, we note another qualitative difference between the two methods for calculating fractional populations: The ENS-LDA values of E_f are above the exact ones, but the FOO-LDA values are below. This behavior can be traced back to an increased

delocalization of the LDA-FOO densities when compared to ENS (see Fig. 4), which in turn leads to an increased magnitude for the (negative) electron–nuclear interaction energy in FOO. This observation agrees with our analysis in Sec. II C.

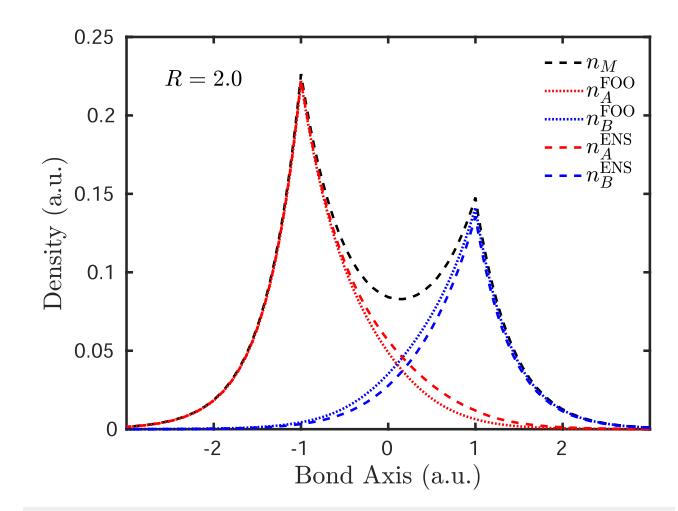


FIG. 4. Fragment densities of the one-electron model molecule $AB^{+0.9}$ ($Z_A = 1$ and $Z_B = 0.9$) along the bond axis at optimal electron populations with FOO + LDA and ENS + LDA when the internuclear distance is R = 2.0 a.u.

Setting the bond mid-point as the origin, we define fragment electronic dipole moments as $\mathbf{p}_{\alpha} = \int \mathbf{r} n_{\alpha}(\mathbf{r}) d\mathbf{r}$. Then, $\mathbf{p}_{A}^{FOO} = 0.4219 > 0.3962 = \mathbf{p}_{A}^{ENS}$ and $|\mathbf{p}_{B}^{FOO}| = |-0.2942| > |-0.2685| = |\mathbf{p}_{B}^{ENS}|$. Clearly, the FOO fragments are more polarized than the ENS fragments.

For a given approximation to the XC energy functional (in this case LDA), P-DFT produces the same total energy and density that one would get from a molecular KS-DFT calculation. FOO and ENS partition the same total density differently as can be seen in Fig. 4, but when the internuclear distance grows beyond the equilibrium separation, the density in this internuclear region becomes exponentially small and the differences in fragment densities produced by FOO and ENS also become correspondingly small. At the dissociation limit, these differences tend to zero and FOO and ENS yield the same dissociation error in this limit.

B. Two electrons: Model of a two-electron molecule $\mathbf{A}\mathbf{B}^{+\delta}$

We now add one more electron and allow both electrons to fully interact with each other and with the two nuclei. To keep the system bound in the LDA, this time we fix $Z_B = 1$ and let $Z_A \in [1,2]$, so we vary $\delta \equiv Z_A - Z_B$ from zero (H₂) to one (HeH⁺). While the fragment electron populations were always non-integers for the previous one-electron diatomic molecule, we will show here that, for a range of δ , the electron–electron interaction can make the fragments acquire strictly integer populations, i.e., $N_A^* = N_B^* = 1$.

Our goal in this section is to compare the performance of ENS and FOO for the LDA, so the "reference data" needed here is simply that of a molecular LDA calculation. We consider two separation channels in the LDA: *channel* I—when $1 \le Z_A < 1.607$, the separated state is one hydrogen atom and a one-electron atom whose nuclear charge is Z_A , and *channel* II—when $1.607 < Z_A \le 2$, the separated state is one proton and a two-electron atom with nuclear charge Z_A .

We begin by finding the optimum populations by identifying the value of N_A at which the electronegativities of A and B become equal. However, special care is needed here as the ENS electronegativities are undefined at strictly integer populations, but one can define left- (right-) electronegativities, χ_{α}^{-} (χ_{α}^{+}), as the left (right) limits of $-\frac{\partial \tilde{E}_{\alpha}[n_{\alpha}]}{\partial n_{\alpha}(\mathbf{r})}$. Figure 5 shows that fragment electronegativities are discontinuous at $N_A = 1$. When $Z_A = 1.1$, $N_A = 1$ is the global minimizer of E_f . However, when $Z_A = 1.45$, $N_A = 1$ is no longer the global minimizer (the inset in the lower right panel of Fig. 5 shows that $N_A^* = 1.1$ leads to a slightly lower E_f than $N_A = 1.0$). How can one know if the global minimizer of E_f will involve integer or fractional populations? Fig. 6 provides the answer. The left and right electronegativities at $N_A = 1$ are shown here as a function of Z_A . We find that when $1 \le Z_A \le 1.422$, the intersection of $\left[-\chi_A^-, -\chi_A^+\right]$ and $\left[-\chi_B^+, -\chi_B^-\right]$ is not empty (shaded area in Fig. 6), and $N_A = 1$ is the global minimizer of E_f . Otherwise, $N_A = 1$ is no longer the global minimizer of E_f , and the optimum populations become fractional, in agreement with the electronegativity equalization principle.

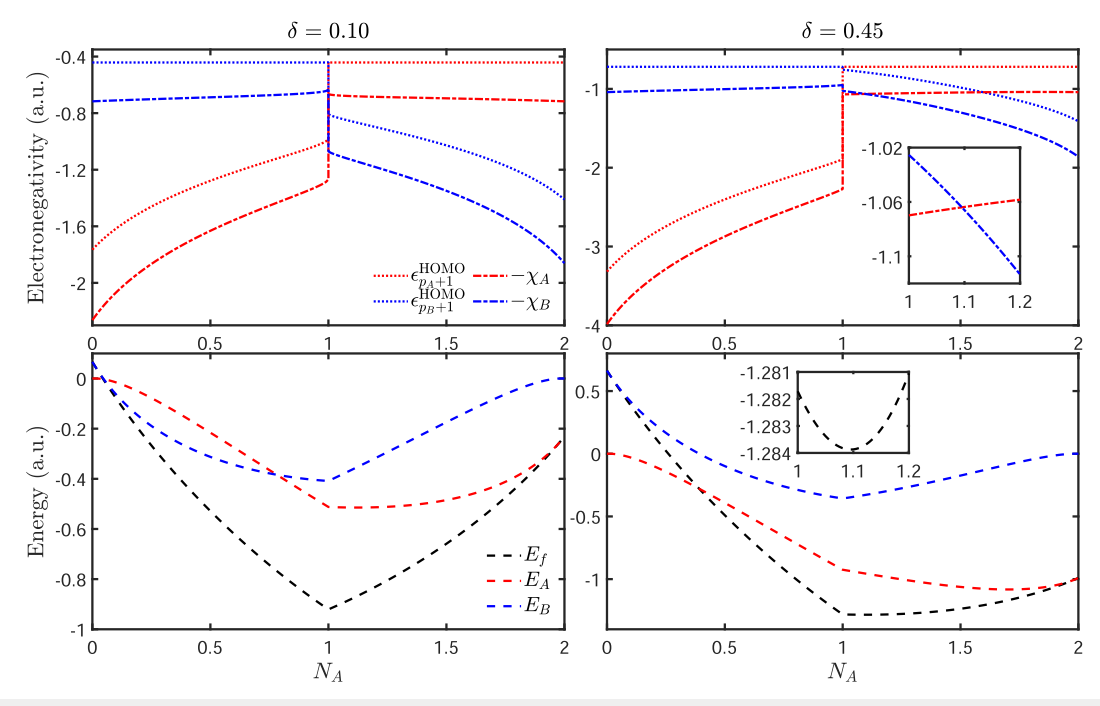


FIG. 5. Top left: Negative electronegativities of fragments and HOMO energies as a function of N_A for the two-electron molecule AB $^{+\delta}$ of Sec. III B ($Z_A = 1.1$ and $Z_B = 1$) with LDA and ENS at internuclear distance R = 1.446 a.u. and $\varepsilon_M^{\text{HOMO}} = -0.4419$ a.u. Bottom left: Fragment energies and their sum as a function of N_A . The top and bottom right panels are the same as the top and bottom left panels, respectively, but with $Z_A = 1.45$.

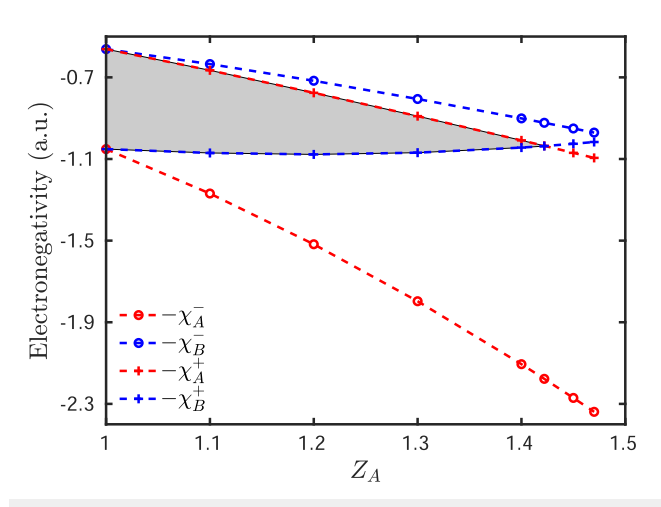


FIG. 6. ENS-LDA left and right electronegativities of fragments A and B as a function of Z_A for the two-electron model molecule AB^{+ δ} of Sec. III B ($Z_B = 1$) at internuclear distance R = 1.446 a.u. when $N_A = N_B = 1$. The shaded area corresponds to the range of Z_A for which the optimum fragment populations are strictly integers.

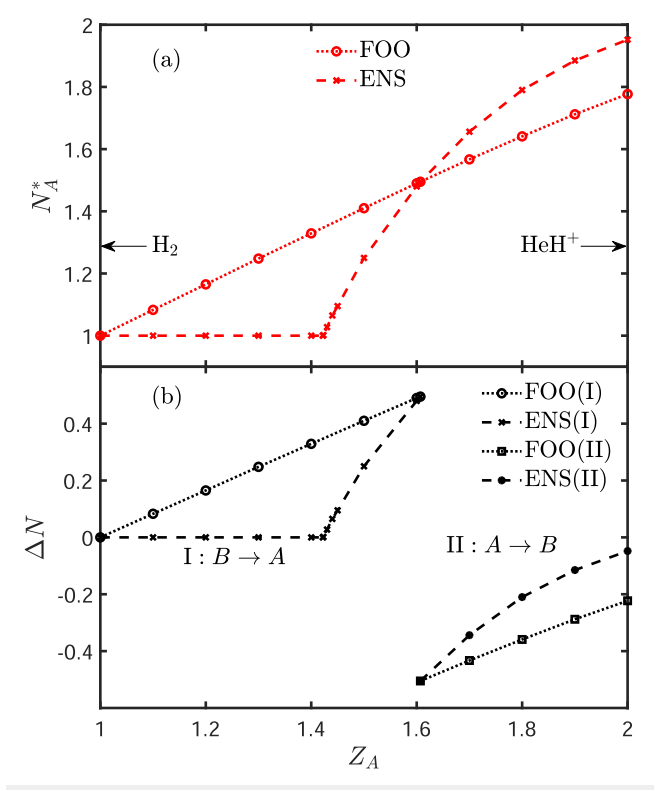


FIG. 7. (a) Optimal electron population of fragment A, N_A^* , as a function of Z_A for the two-electron model molecule $AB^{+\delta}$ ($Z_B=1$) with FOO and ENS, at internuclear distance R=1.446 a.u. (b) The number of electrons transferred from fragment B to A, ΔN , as a function of Z_A for the two dissociation channels discussed in the text.

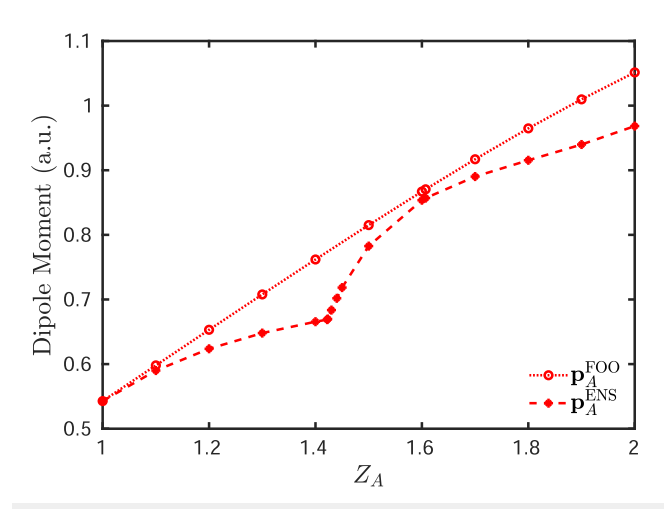


FIG. 8. Electronic dipole moments of fragment A as a function of Z_A for the two-electron model molecule AB^{+ δ} (Z_B = 1) with FOO and ENS.

The FOO electronegativities are well defined when the electron populations are integers. ³⁹ There is no need to define left and right quantities here, as in ENS. The behavior of the $\chi_{\alpha}^{\rm FOO}$ is similar to that of the one-electron electronegativities of Fig. 3.

Figure 7 compares $N_A^*(Z_A)$ from FOO and ENS. While the optimum numbers are non-integers in FOO for the entire range $1 < Z_A \le 2$, they are integers in ENS when $1 < Z_A \le 1.422$ for the reasons mentioned above. Figure 7 also shows that FOO and ENS yield the same N_A^* at $Z_A = 1.607$. This is the critical nuclear charge above which channel II becomes the ground state. To emphasize this point, Fig. 7 shows the number of electrons transferred ΔN for the range $1 < Z_A < 2$, indicating the ground-state dissociation channel in each case. Electrons are transferred from B to A when $Z_A < 1.607$ and from A to B when $Z_A > 1.607$. We note that $|\Delta N|$ is always lower in ENS than in FOO. The ENS fragment dipoles are also always smaller (Fig. 8).

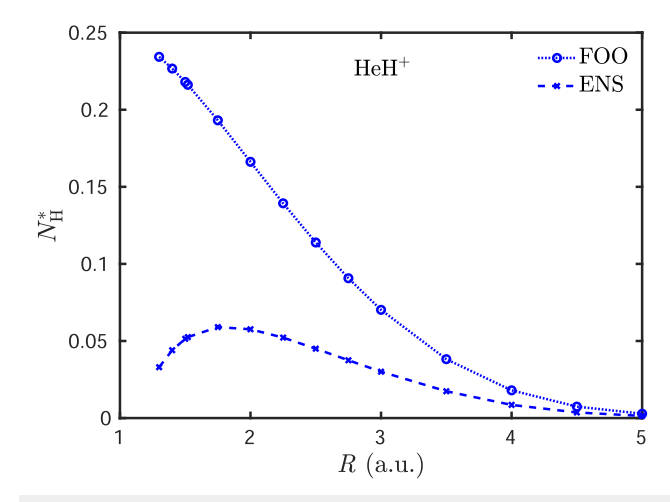


FIG. 9. Optimal electron population of fragment H, $N_{\rm H}^*$, as a function of internuclear distance for HeH $^+$ with FOO and ENS.

1. Dissociation of HeH+

We now compare FOO and ENS results for the optimum number of electrons transferred in HeH $^+$ as the internuclear separation increases from $R \sim 1$ a.u. up to $R \sim 5$ a.u (Fig. 9). The separated state of HeH $^+$ is a helium atom and a proton. The proton is dressed with a small fraction of an electron at finite R and we note that the qualitative behavior of this small fraction $N_{\rm H}^*(R)$ is similar to that observed in the exact case for the one-electron molecule of Sec. III A (Fig. 2): (1) The fraction of an electron reaches a maximum for ENS at $R \sim 1.8$ a.u.; (2) the FOO and ENS values approach each other as R grows; and (3) the electron fraction given by FOO is larger than that given by ENS for all R.

C. Four electrons: Lithium hydride

Finally, we briefly examine the four-electron molecule LiH at its equilibrium separation ($R_{eq} = 3.03$ a.u.). In a previous work,⁵¹ it was speculated that the optimal P-DFT electron populations of the atomic fragments would be non-integers at R_{eq} . However, a recent exact P-DFT calculation³² of a one-dimensional two-electron model of LiH yielded strictly integer populations. Figure 10 shows our LDA P-DFT energies for 3D LiH using both ENS and FOO. We find that, by using ENS, the populations are, indeed, integers, as in the one-dimensional two-electron model.³² Although the densities of Li and H fragments are distorted versions of the corresponding isolated-atom densities (see the H-atom density distortions in Fig. 11), there is no electron transfer between fragments in ENS. However, by using FOO, the fragment electron populations are nonintegers. At the equilibrium internuclear distance, $R_{eq} = 3.03$ a.u., we obtain $N_{\rm Li}^* = 2.663$ and $N_{\rm H}^* = 1.337$. The number of electrons transferred from Li to H is $\Delta N = 0.337$. Just as in the examples of Secs. III A and III B, the number of electrons transferred with the FOO method is larger than with the ENS method (which is just zero in this case). To understand why, we distinguish three zones and note that when the number of electrons in the lithium atom is less than the optimum predicted by FOO (zone 1: $N_{\rm Li}$ < 2.663),

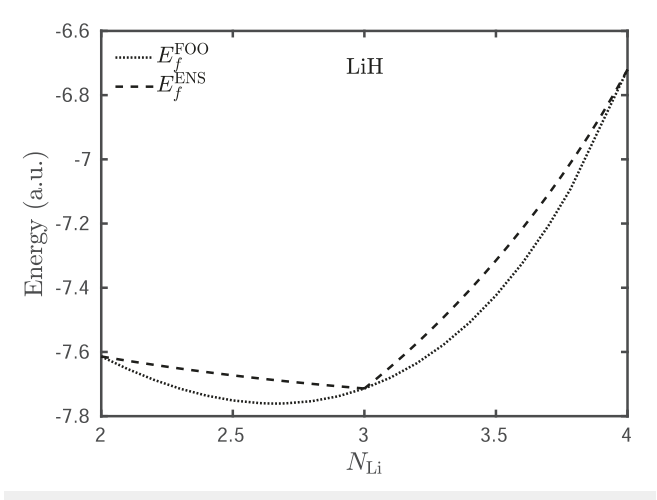


FIG. 10. The sum of fragment energies, $E_{\rm f}$, as a function of N_A for LiH with FOO and ENS at the equilibrium internuclear distance R=3.03 a.u.

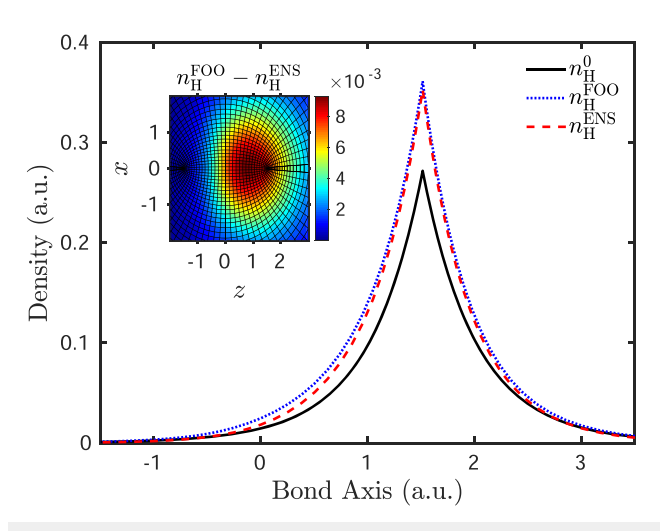


FIG. 11. Optimal electron densities for the H fragment in LiH with FOO and ENS at the equilibrium internuclear distance R = 3.03 a.u.; the solid line corresponds to an isolated hydrogen atom density. The inset shows the difference between the FOO and ENS fragment densities on the xz plane.

then $\varepsilon_{\rm H,FOO}^{\rm HOMO} = \varepsilon_{\rm H,ENS}^{\rm HOMO} = \varepsilon_{\rm LiH}^{\rm HOMO}$. However, when that number is higher than the optimum predicted by ENS (*zone* 2: $N_{\rm Li} > 3.0$), then $\varepsilon_{\rm Li,FOO}^{\rm HOMO} = \varepsilon_{\rm Li,ENS}^{\rm HOMO} = \varepsilon_{\rm LiH}^{\rm HOMO}$. Finally, when $N_{\rm Li}$ is in between those two values (*zone* 3: $2.663 < N_{\rm Li} < 3.0$), then $\varepsilon_{\rm Li,FOO}^{\rm HOMO} = \varepsilon_{\rm H,ENS}^{\rm HOMO} = \varepsilon_{\rm LiH}^{\rm HOMO}$

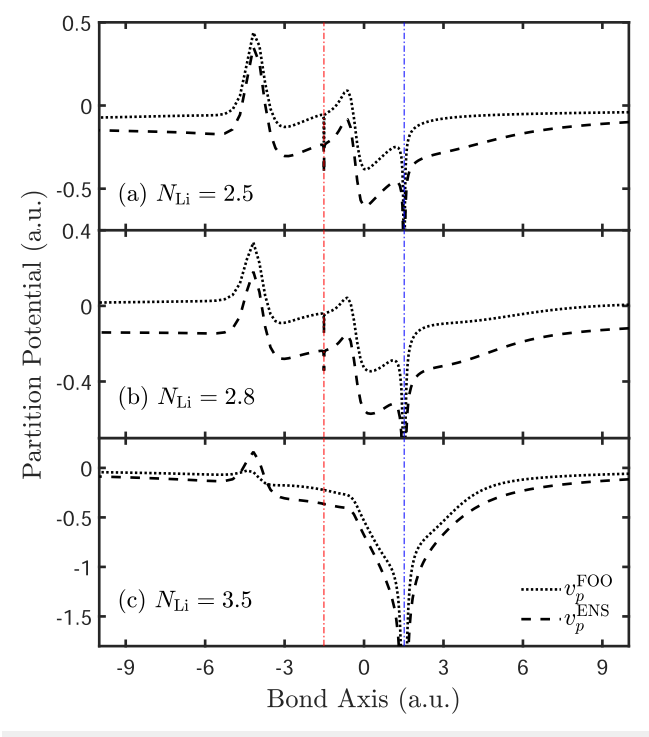


FIG. 12. Partition potential along the bond axis for LiH with FOO and ENS at the equilibrium internuclear distance R=3.03 a.u. when (a)–(c) $N_{\rm Li}=2.5, 2.8$, and 3.5. The red (blue) dashed-dotted straight lines indicate the positions of the Li (H) nuclei

and $\varepsilon_{\text{Li,ENS}}^{\text{HOMO}} < \varepsilon_{\text{LiH}}^{\text{HOMO}}$. Our analysis of Sec. II C then implies that $v_p^{\text{ENS}}(\mathbf{r})$ is deeper than $v_p^{\text{FOO}}(\mathbf{r})$ (Fig. 12) and $E_f^{\text{ENS}} > E_f^{\text{FOO}}$ (Fig. 10). It can be seen in Fig. 12 that the partition potential does not change qualitatively when $N_{\rm Li}$ crosses from zone 1 to zone 3, but there are major qualitative changes when it crosses to zone 2.

IV. CONCLUDING REMARKS

By treating fragment electron populations as variables in P-DFT calculations, we have shown how to find optimal populations via two alternative methods, one that involves fractional orbital occupations (FOO) and another that makes use of ensemble averages (ENS). The optimal populations are found in both cases when the sum of fragment energies E_f reaches its global minimum and all fragment electronegativities become equal. At that optimum, a value for the charge transferred between two fragments can be assigned unambiguously even at finite internuclear separations.

Through the formal analysis of Sec. II and the explicit numerical calculations of Sec. III, we have revealed differences between FOO and ENS that had not been observed in previous studies: (1) Although both methods lead to the same molecular densities and energies, the fragment densities of hetero-nuclear diatomic molecules can be significantly different, with the FOO method consistently yielding a larger fraction of an electron transferred from donor to acceptor, at least when the LDA is employed; (2) the FOO fragment dipole moments are observed to provide an upper bound to the corresponding ENS dipole moments; (3) the ENS partition potentials are deeper than the corresponding FOO partition potentials; and (4) accordingly, $E_f^{\rm ENS} > E_f^{\rm FOO}$ and $E_p^{\rm ENS} < E_p^{\rm FOO}$. Although a general proof of these observations is far beyond

the scope of this work, we suspect that FOO will generally transfer more electrons than ENS: When the nuclei are far enough apart, the effect of the partition potential on the fragment densities is negligible and the ENS fragment energies vary linearly with electron number. Since this occurs for both fragments, and since the FOO energies are observed to be convex functions of the electron number, the sum of fragment energies is expected to be lower in FOO than in ENS. The situation is less clear at finite internuclear separations R, but the small deviations from linearity detected for ENS even at small R (certainly at equilibrium) suggest that the conclusions will remain valid, in general, at finite *R*.

With appropriate approximations to the partition energy functional, P-DFT has been recently shown to overcome staticcorrelation and delocalization errors when stretching homonuclear diatomic molecules.8 Also, for homonuclear diatomic molecules, a proposed "covalent" approximation for the non-additive noninteracting kinetic energy shows promising results for orbital-free calculations.²⁹ An extension of these approximations to the ionic case and, more generally, to chemical bonds connecting inequivalent fragments, would be desirable. This extension will require choosing a method to treat fractional populations. Although both FOO and ENS methods are valid candidates, the results of this work point to the advantages of each method in different cases: The observation that ENS fragment densities are less distorted than FOO densities upon formation of a chemical bond is a significant advantage for ENS, both conceptually and computationally. Conceptually, it is pleasing to have fragments-in-molecules that are minimally distorted from their isolated counterparts. Computationally, although each iteration of the P-DFT equations involves two integer-number calculations (vs only one in FOO), the minimal distortion of the isolated input densities leads to a faster convergence that will benefit future applications. On the other hand, when using the LDA on polar diatomic molecules at their equilibrium internuclear separations, the FOO method has the advantage that it always leads to fractional populations in line with the chemist's intuition that polar molecules are composed of fragments with fractional formal charges.

ACKNOWLEDGMENTS

The authors thank Yan Oueis for valuable discussions. This work was supported by the National Science Foundation under Grant No. CHE-1900301.

AUTHOR DECLARATIONS

Conflict of Interest

The authors have no conflicts to disclose.

DATA AVAILABILITY

The data that support the findings of this study are available from the corresponding author upon reasonable request.

REFERENCES

- ¹P. Hohenberg and W. Kohn, "Inhomogeneous electron gas," Phys. Rev. 136, B864-B871 (1964).
- ²W. Kohn and L. J. Sham, "Self-consistent equations including exchange and correlation effects," Phys. Rev. 140, A1133-A1138 (1965).
- ³R. G. Parr and Y. Weitao, Density-Functional Theory of Atoms and Molecules (Oxford University Press, New York, 1989).
- ⁴A. J. Cohen, P. Mori-Sánchez, and W. Yang, "Challenges for density functional theory," Chem. Rev. 112, 289-320 (2012).
- ⁵ A. J. Cohen, P. Mori-Sánchez, and W. Yang, "Insights into current limitations of density functional theory," Science 321, 792-794 (2008).
- ⁶M. R. Pederson, A. Ruzsinszky, and J. P. Perdew, "Communication: Selfinteraction correction with unitary invariance in density functional theory," J. Chem. Phys. 140, 121103 (2014).
- ⁷E. Kraisler and L. Kronik, "Elimination of the asymptotic fractional dissociation problem in Kohn-Sham density-functional theory using the ensemblegeneralization approach," Phys. Rev. A 91, 032504 (2015).
- ⁸J. Nafziger and A. Wasserman, "Fragment-based treatment of delocalization and static correlation errors in density-functional theory," J. Chem. Phys. 143, 234105 (2015).
- ⁹C. Li, X. Zheng, N. Q. Su, and W. Yang, "Localized orbital scaling correction for systematic elimination of delocalization error in density functional approximations," Natl. Sci. Rev. 5, 203-215 (2018).
- ¹⁰J. P. Perdew, "Artificial intelligence 'sees' split electrons," Science 374,
- ¹¹ J. Kirkpatrick, B. McMorrow, D. H. P. Turban, A. L. Gaunt, J. S. Spencer, A. G. D. G. Matthews, A. Obika, L. Thiry, M. Fortunato, D. Pfau, L. R. Castellanos,

- S. Petersen, A. W. R. Nelson, P. Kohli, P. Mori-Sánchez, D. Hassabis, and A. J. Cohen, "Pushing the frontiers of density functionals by solving the fractional electron problem," Science **374**, 1385–1389 (2021).
- ¹²P. Mori-Sánchez, A. J. Cohen, and W. Yang, "Localization and delocalization errors in density functional theory and implications for band-gap prediction," Phys. Rev. Lett. 100, 146401 (2008).
- ¹³ M. H. Cohen and A. Wasserman, "On hardness and electronegativity equalization in chemical reactivity theory," J. Stat. Phys. 125, 1121–1139 (2006).
- ¹⁴R. Tang, J. Nafziger, and A. Wasserman, "Fragment occupations in partition density functional theory," Phys. Chem. Chem. Phys. 14, 7780–7786 (2012).
- ¹⁵E. Fabiano, S. Laricchia, and F. D. Sala, "Frozen density embedding with non-integer subsystems' particle numbers," J. Chem. Phys. 140, 114101 (2014).
- ¹⁶ A. Schulz and C. R. Jacob, "Description of intermolecular charge transfer with subsystem density-functional theory," J. Chem. Phys. 151, 131103 (2019).
- ¹⁷Q. Sun and G. K.-L. Chan, "Quantum embedding theories," Acc. Chem. Res. 49, 2705–2712 (2016).
- ¹⁸A. Wasserman and M. Pavanello, "Quantum embedding electronic structure methods," Int. J. Quantum Chem. **120**, e26495 (2020).
- ¹⁹M. H. Cohen and A. Wasserman, "On the foundations of chemical reactivity theory," J. Phys. Chem. A 111, 2229–2242 (2007).
- ²⁰P. Elliott, K. Burke, M. H. Cohen, and A. Wasserman, "Partition density-functional theory," Phys. Rev. A 82, 024501 (2010).
- ²¹ J. Nafziger and A. Wasserman, "Density-based partitioning methods for ground-state molecular calculations," J. Phys. Chem. A 118, 7623–7639 (2014).
 ²² T. A. Wesolowski and A. Warshel, "Frozen density functional approach for ab
- ²²T. A. Wesolowski and A. Warshel, "Frozen density functional approach for ab initio calculations of solvated molecules," J. Phys. Chem. 97, 8050–8053 (1993).
- ²³C. R. Jacob and J. Neugebauer, "Subsystem density-functional theory," Wiley Interdiscip. Rev.: Comput. Mol. Sci. 4, 325–362 (2014).
- ²⁴T. A. Wesolowski, S. Shedge, and X. Zhou, "Frozen-density embedding strategy for multilevel simulations of electronic structure," Chem. Rev. 115, 5891–5928 (2015).
- ²⁵P. Cortona, "Self-consistently determined properties of solids without band-structure calculations," Phys. Rev. B 44, 8454–8458 (1991).
- ²⁶C. Huang, M. Pavone, and E. A. Carter, "Quantum mechanical embedding theory based on a unique embedding potential," J. Chem. Phys. **134**, 154110 (2011).
- ²⁷C. Huang and E. A. Carter, "Potential-functional embedding theory for molecules and materials," J. Chem. Phys. 135, 194104 (2011).
- ²⁸J. P. Perdew, R. G. Parr, M. Levy, and J. L. Balduz, "Density-functional theory for fractional particle number: Derivative discontinuities of the energy," Phys. Rev. Lett. **49**, 1691–1694 (1982).
- ²⁹K. Jiang, J. Nafziger, and A. Wasserman, "Constructing a non-additive non-interacting kinetic energy functional approximation for covalent bonds from exact conditions," J. Chem. Phys. **149**, 164112 (2018).
- ³⁰ M. H. Cohen, A. Wasserman, R. Car, and K. Burke, "Charge transfer in partition theory," J. Phys. Chem. A 113, 2183–2192 (2009).

- ³¹P. Elliott, M. H. Cohen, A. Wasserman, and K. Burke, "Density functional partition theory with fractional occupations," J. Chem. Theory Comput. 5, 827–833 (2009).
- ³²Y. Oueis and A. Wasserman, "Exact partition potential for model systems of interacting electrons in 1-D," Eur. Phys. J. B 91, 247 (2018).
- ³³ J. Nafziger, K. Jiang, and A. Wasserman, "Accurate reference data for the nonadditive, noninteracting kinetic energy in covalent bonds," J. Chem. Theory Comput. 13, 577–586 (2017).
- ³⁴R. S. Mulliken, "Electronic population analysis on LCAO–MO molecular wave functions. I," J. Chem. Phys. **23**, 1833–1840 (1955).
- ³⁵F. L. Hirshfeld, "Bonded-atom fragments for describing molecular charge densities," Theor. Chim. Acta 44, 129–138 (1977).
- ³⁶ A. E. Reed, R. B. Weinstock, and F. Weinhold, "Natural population analysis," J. Chem. Phys. 83, 735–746 (1985).
- ³⁷R. F. W. Bader, Atoms in Molecules: A Quantum Theory (Oxford University Press, New York, 1990).
- 38 B. Rousseau, A. Peeters, and C. Van Alsenoy, "Atomic charges from modified Voronoi polyhedra," J. Mol. Struct.: THEOCHEM 538, 235–238 (2001).
- ³⁹J. F. Janak, "Proof that $\frac{\partial e}{\partial n_i} = \varepsilon$ in density-functional theory," Phys. Rev. B **18**,
- 7165–7168 (1978). ⁴⁰R. P. Iczkowski and J. L. Margrave, "Electronegativity," J. Am. Chem. Soc. **83**,
- 3547–3551 (1961).

 41 H. Englisch and R. Englisch, "Exact density functionals for ground-state
- energies. I. General results," Phys. Status Solidi B 123, 711–721 (1984).

 42 H. Englisch and R. Englisch, "Exact density functionals for ground-state
- energies II. Details and remarks," Phys. Status Solidi B **124**, 373–379 (1984). ⁴³S. R. P. G. Ripka, J.-P. Blaizot, and G. Ripka, *Quantum Theory of Finite Systems* (MIT Press, 1986).
- ⁴⁴M. Levy, J. P. Perdew, and V. Sahni, "Exact differential equation for the density and ionization energy of a many-particle system," Phys. Rev. A 30, 2745–2748 (1984)
- ⁴⁵A. J. Cohen and P. Mori-Sánchez, "Dramatic changes in electronic structure revealed by fractionally charged nuclei," J. Chem. Phys. 140, 044110 (2014).
- ⁴⁶J. W. Furness, R. Zhang, and J. Sun, "A paradigm system for strong correlation and charge transfer competition," arXiv:2103.03178 [physics] (2021).
- ⁴⁷A. D. Becke, "Numerical Hartree-Fock-Slater calculations on diatomic molecules," J. Chem. Phys. **76**, 6037–6045 (1982).
- ⁴⁸M. A. L. Marques, M. J. T. Oliveira, and T. Burnus, "LIBXC: A library of exchange and correlation functionals for density functional theory," Comput. Phys. Commun. **183**, 2272–2281 (2012).
- ⁴⁹R. P. Feynman, M. Sands, and R. B. Leighton, "The Feynman lectures on physics," in *The New Millennium Edition: Quantum Mechanics*, New Millennium ed. (Basic Books, New York, 2011), Vol. 3.
- ⁵⁰J. P. Perdew and A. Zunger, "Self-interaction correction to density-functional approximations for many-electron systems," Phys. Rev. B 23, 5048–5079 (1981).
- ⁵¹J. Nafziger, Q. Wu, and A. Wasserman, "Molecular binding energies from partition density functional theory," J. Chem. Phys. **135**, 234101 (2011).